Swarthmore College

Works

5-20-2011

Processing The Interspecies Quorum-Sensing Signal Autoinducer-2 (AI-2) Characterization Of Phospho-(S)-4,5-Dihydroxy-2,3-Pentanedione Isomerization By LsrG Protein

J. C. Marques

P. Lamosa

Caitlin Elizabeth Russell , '11

See next page for additional authors

Follow this and additional works at: https://works.swarthmore.edu/fac-chemistry

Part of the Biochemistry Commons

Let us know how access to these works benefits you

Recommended Citation

Authors

J. C. Marques; P. Lamosa; Caitlin Elizabeth Russell , '11; R. Ventura; C. D. Maycock; M. F. Semmelhack; Stephen T. Miller; and K. B. Xavier

Processing the Interspecies Quorum-sensing Signal Autoinducer-2 (AI-2)

CHARACTERIZATION OF PHOSPHO-(S)-4,5-DIHYDROXY-2,3-PENTANEDIONE ISOMERIZATION BY LsrG PROTEIN*[S]

João C. Marques[‡§]**, Pedro Lamosa**[§]**, Caitlin Russell**[¶]**, Rita Ventura**[§]**, Christopher Maycock**[§∥]**, Martin F. Semmelhack**[**]**, Stephen T. Miller**[¶1]**, and Karina B. Xavier**[‡§2]

From the ‡*Instituto Gulbenkian de Ciência and the* §*Instituto de Tecnologia Química e Biológica, 2780 Oeiras, Portugal, the* ¶*Department of Chemistry and Biochemistry, Swarthmore College, Swarthmore, Pennsylvania 19081, the* ∥*Faculdade de Ciências da Universidade de Lisboa, Departamento de Química e Bioquímica, 1749 Lisboa, Portugal, and the* **Department of Chemistry, Princeton University, Princeton, New Jersey 08544*

The molecule (S)-4,5-dihydroxy-2,3-pentanedione (DPD) is produced by many different species of bacteria and is the precursor of the signal molecule autoinducer-2 (AI-2). AI-2 mediates interspecies communication and facilitates regulation of bacterial behaviors such as biofilm formation and virulence. A variety of bacterial species have the ability to sequester and process the AI-2 present in their environment, thereby interfering with the cell-cell communication of other bacteria. This process involves the AI-2-regulated *lsr* operon, comprised of the Lsr transport system that facilitates uptake of the signal, a kinase that phosphorylates the signal to phospho-DPD (P-DPD), and enzymes (like LsrG) that are responsible for processing the phosphorylated signal. Because P-DPD is the intracellular inducer of the *lsr* operon, enzymes involved in P-DPD processing impact the levels of Lsr expression. Here we show that LsrG catalyzes isomerization of P-DPD into 3,4,4-trihydroxy-2-pentanone-5-phosphate. We present the crystal structure of LsrG, identify potential catalytic residues, and determine which of these residues affects P-DPD processing *in vivo* and *in vitro*. We also show that an *lsrG* deletion mutant accumulates at least 10 times more P-DPD than wild type cells. Consistent with this result, we find that the *lsrG* mutant has increased expression of the *lsr* operon and an altered profile of AI-2 accumulation and removal. Understanding of the biochemical mechanisms employed by bacteria to quench signaling of other species can be of great utility in the development of therapies to control bacterial behavior.

Many bacteria regulate gene expression as a function of the density of the population. This process, called quorum sensing, enables these organisms to coordinate behaviors that are most beneficial when cells are working in unison (1, 2). Quorum sensing is mediated by signal molecules called autoinducers. One autoinducer (Autoinducer-2 (AI-2)[3]) is produced by many species of bacteria and can facilitate interspecies cell-cell signaling (3–5). AI-2 is produced by the enzyme LuxS, which synthesizes (S)-4,5-dihydroxy-2,3-pentanedione (DPD; Fig. 1A, **1**), the linear form of a set of interconverting molecules with AI-2 activity (6–8). AI-2 (or its synthase LuxS) has been shown to regulate important bacterial behaviors such as biofilm formation and the production of virulence factors (4, 5, 9, 10). Thus, one strategy for controlling these behaviors is to control the concentration (or availability) of AI-2. We have previously shown that certain bacteria can employ this strategy by processing AI-2 and thus quenching interspecies signaling (11). These bacteria include most members from the Enterobacteriaceae family (like the commensal *Escherichia coli* K12 and the pathogens *E. coli* O157 and *Salmonella typhimurium*) but also more distantly related bacteria such as the plant symbiont *Sinorhizobium meliloti* and the pathogen *Bacillus anthracis* (12).

In these bacteria, AI-2 controls the expression of a system (named Lsr for luxS-regulated) capable of processing both endogenous and exogenous AI-2 (13–16). Using the Lsr system, these bacteria remove AI-2 from the environment and, thus, eliminate the ability of others to utilize AI-2 to regulate their behaviors (11). Upon internalization by the Lsr transporter, AI-2 is phosphorylated to phospho-DPD (P-DPD, Fig. 1A, **2**) by the kinase LsrK (17, 18). P-DPD is the inducer of the Lsr system and acts by binding to and inactivating the transcriptional repressor LsrR (18, 19). Thus, P-DPD triggers the induction of the Lsr system, causing a fast uptake of extracellular AI-2 and processing of internalized AI-2. Therefore, it is expected that

[3] The abbreviations used are: AI-2, autoinducer-2; DPD, (S)-4,5-dihydroxy-2,3-pentanedione; P-DPD, phospho-DPD; Lsr, *luxS* regulated; P-TPO, 3,4,4-trihydroxy-2-pentanone-5-phosphate; P-HPD, 3-hydroxy-2,4-pentadione-5-phosphate; P-TetraPO, 3,3,4,4-tetrahydroxy-2-pentanone-5-phosphate; HSQC, heteronuclear single quantum coherence; HMBC, heteronuclear multiple bond connectivity; Cm, chloramphenicol; r.m.s.d., root mean square deviation.
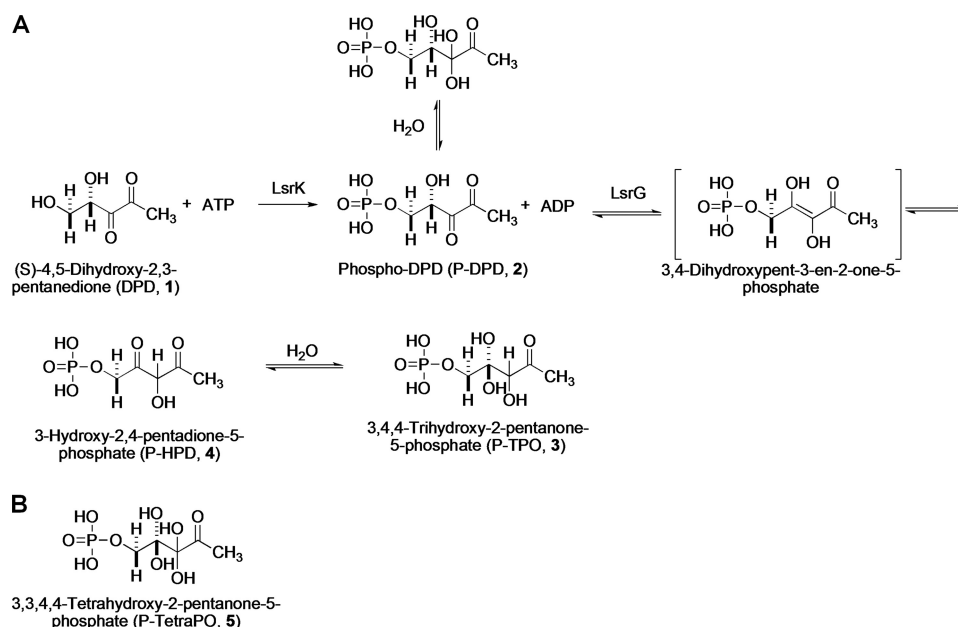
FIGURE 1. **Model of the proposed reaction pathway for P-DPD isomerization by LsrG.** *A*, in the presence of ATP and reducing agent DPD (**1**) is phosphorylated by LsrK, producing phospho-DPD (*P-DPD*, **2**). The hydrated form of P-DPD is also shown because this is the major form of P-DPD detected under our reaction conditions. LsrG converts P-DPD into 3,3,4-trihydroxy-2-pentanone-5-phosphate (*P-TPO*, **3**) by catalyzing the tautomerization of P-DPD into 3-hydroxy-2,4-pentadione-5-phosphate (*P-HPD*, **4**) via a transient 3,4-enediol intermediate and subsequent hydration of the carbon 4-ketone group. It is likely that the hydrated (**3**) and non-hydrated (**4**) forms exist in equilibrium. *B*, in the presence of oxygen P-TPO is oxidized non-enzymatically to 3,3,4,4-tetrahydroxy-2-pentanone-5-phosphate (*P-TetraPO*, **5**). For clarity and easy description of structural differences, the numbering of the carbons of all the compounds is based on the numbering of DPD.

every enzyme acting on P-DPD has a significant impact on AI-2 internalization and, hence, on AI-2-dependent interspecies cell-cell signaling. We have previously shown that LsrG is one of the enzymes involved in processing of P-DPD (18). We showed that under aerobic conditions, *in vitro* incubation of LsrG with P-DPD results in the production of phosphoglycolate as well as multiple other compounds that accumulate to low levels. Neither the catalytic mechanism of LsrG nor the other compounds produced in the LsrG reaction were identified.

Here, we characterize the enzymatic reaction catalyzed by LsrG. We show that LsrG catalyzes the conversion of P-DPD to the isomer 3,4,4-trihydroxy-2-pentanone-5-phosphate (P-TPO, Fig. 1*A*, **3**) and propose the reaction that leads to the formation of this compound (Fig. 1*A*). Under reducing conditions (*i.e.* the conditions typically found in the cytoplasm) P-TPO and the non-hydrated form of this compound (3-hydroxy-2,4-pentadi-one-5-phosphate (P-HPD, Fig. 1*A*, **4**) are stable and do not degrade readily. However, under oxidizing conditions, P-TPO and P-HPD are oxidized to a compound we identify as 3,3,4,4-tetrahydroxy-2-pentanone-5-phosphate (P-TetraPO, Fig, 1*B*, **5**), which in turn degrades into phosphoglycolate and other smaller molecules produced in minor concentrations.

We also present the crystal structure of LsrG. LsrG shares a fold with proteins belonging to the cofactor-independent monooxygenase family (20, 21). Interestingly, although the location of the LsrG active site is the same as in monooxygenases, the identity of the residues in the active site is not highly conserved. The LsrG structure has allowed us to identify potential catalytic residues, identifications that were then validated *in vitro* and *in vivo*. Finally, to determine the role of LsrG in the process of interference with AI-2 mediated signaling, we measured the impact of LsrG mutants on the intracellular accumu-

lation of P-DPD, on the expression of the *lsr* operon, and on extracellular AI-2 accumulation/removal. Characterization of LsrG and the role it plays in AI-2 processing is essential for understanding how organisms that possess the Lsr system act to quench AI-2 signaling. This knowledge opens the door to the potential exploitation of these mechanisms as a means for controlling quorum sensing.

EXPERIMENTAL PROCEDURES

Overexpression and Purification of LsrG

E. coli LsrG was cloned into the pProEXHTb plasmid for overexpression as an N-terminal His$_6$-tagged fusion protein. After transformation of the plasmid into *E. coli* strain BL21, cultures were grown in Luria-Bertani medium (Sigma) with shaking at 37 °C to an A_{595} of 0.3. The temperature was lowered to 22 °C, and growth continued until an A_{595} of 0.9 was reached. Protein expression was induced by the addition of 0.1 mM iso-propyl-β-D-thiogalactopyranoside. After 15 h of growth at 22 °C with shaking post-induction, bacteria were harvested by centrifugation. Cells were resuspended in 50 mM NaH$_2$PO$_4$, pH 8.0, 300 mM NaCl, 10 mM imidazole, 1.4 mM β-mercaptoetha-nol, 2.5 μg ml^{-1} DNase, 2.5 μg ml^{-1} leupeptin, and 2.5 μg ml^{-1} aprotinin. Cells were lysed using a M-110Y Microfluidizer (Microfluidics). Lysates were clarified via centrifugation.

The His$_6$-LsrG fusion protein was purified by affinity chromatography using nickel-nitrilotriacetic acid-agarose (Qiagen). After application of the lysate, the columns were washed with 50 mM NaH$_2$PO$_4$, pH 8.0, 300 mM NaCl, 20 mM imidazole, and 1.4 mM β-mercaptoethanol. The fusion protein was eluted from the columns using 50 mM NaH$_2$PO$_4$, pH 8.0, 300 mM NaCl, 250 mM imidazole, and 1.4 mM β-mercaptoethanol. Protein-con-

taining fractions were pooled. The pooled protein was buffer swapped into 25 mM Tris, pH 8.0, 50 mM NaCl, and 1 mM dithiothreitol by size exclusion chromatography using a G25 column (GE Healthcare). The protein was then purified by ion exchange chromatography in the new buffer using a SourceQ column (GE Healthcare) with a gradient of 0 to 1 M NaCl.

Fusion protein with the His_6 tag to be left on was then subjected to size exclusion chromatography on a Superdex 75 column (GE Healthcare) and eluted in 25 mM Tris, pH 8.0, 150 mM NaCl, and 1 mM dithiothreitol. The protein was concentrated to 3.0 mg ml^{-1}.

For the LsrG protein, where the His_6 tag was removed, 1 mg of His_6-tobacco etch virus protease per 30 mg of His_6-LsrG fusion protein was added to the post-ion exchange His_6-LsrG. The solution was incubated overnight at 22 °C. The tag and protease were removed by passing the solution over nickel-nitrilotriacetic acid resin. LsrG was eluted with 50 mM NaH_2PO_4, pH 8.0, 300 mM NaCl, 20 mM imidazole, and 1.4 mM β-mercaptoethanol, and protein-containing fractions were pooled. LsrG was then buffer-swapped into 25 mM Tris, pH 8.0, 150 mM NaCl, and 1 mM dithiothreitol by size exclusion chromatography using a Superdex 75 column (GE Healthcare). The purified protein was concentrated to 3.1 mg ml^{-1}.

Four LsrG point mutants (E54A, H65A, N25A, and H70A) were created using the QuikChange Lightning kit (Agilent) per the manufacturer's instructions using primers designed using the QuikChange Primer Design tool. Mutations were confirmed by sequencing, and mutant plasmids were transformed into *E. coli* strain BL21. Mutant protein was expressed and purified, leaving the His_6-tag on, as described above.

DPD Synthesis and Preparation

DPD protected with a cyclohexylidene group was chemically synthesized by the recently developed method as reported in Ascenso *et al.* (22) and dissolved in water to 10 mM. The cyclohexylidene-protecting group was removed with acidic Dowex 50WX8 resin (100 mg ml^{-1} of sample) also as reported previously (22). Deprotected DPD was then neutralized with a final concentration of 30 mM potassium phosphate buffer, pH 7.2. The released cyclohexanone was removed by liquid-liquid extraction with an equal volume of deuterated chloroform. Removal of cyclohexanone is essential to facilitate assignment of the resonances in the methyl region of the NMR spectra. To determine the final concentration of DPD, quantification was performed by ^{1}H NMR using formate as an internal concentration standard.

NMR Spectroscopy

Unless otherwise stated, all spectra were acquired on a Bruker AVANCE III 800 spectrometer (Bruker, Rheinstetten, Germany) working at a proton operating frequency of 800.33 MHz, equipped with a four-channel 5-mm inverse detection probe head with pulse-field gradients along the Z axis. Spectra were run at 4 °C (to avoid compound degradation) using standard Bruker pulse programs. ^{1}H and ^{13}C chemical shifts were referenced to 3-(trimethylsilyl)propane sulfonic acid. ^{31}P chemical shifts were referenced to external 85% phosphoric acid. Standard Bruker pulse programs were used to acquire the

heteronuclear ^{13}C,^{1}H two-dimensional correlation spectra. In the ^{13}C,^{1}H heteronuclear single quantum coherence (HSQC) spectrum, a delay of 3.45 ms was used for evolution of $^1J_{CH}$, whereas a delay of 62.5 ms was used for the ^{1}H,^{31}P correlation spectra. In the heteronuclear multiple bond connectivity (HMBC) spectrum a delay of 73.5 ms was used for evolution of long range couplings. In the HSQC type spectra, proton decoupling was achieved using the GARP4 sequence (23). For the enzyme kinetics determinations, spectra were acquired on a Bruker AVANCE II 500 spectrometer (Bruker) equipped with a 5-mm broadband inverse detection probe head, working at 30 °C with a proton operating frequency of 500.43 MHz. Typically, ^{1}H NMR spectra were acquired with water presaturation using a 60° flip angle and a repetition delay of 5.23 s. The same conditions were used to analyze the cell extracts, but spectra were collected at 4 °C. For quantification purposes formate was added as an internal concentration standard, and an extra relaxation delay of 30 s was used. All samples contained a mixture of D_2O/H_2O with 5% D_2O. For the identification of P-HPD, the correlation spectra were performed in 100% D_2O; in this case, the LsrG reaction was performed with P-DPD that had been lyophilized and was suspended in D_2O before the addition of LsrG.

In Vitro Enzyme Assays

LsrK Reaction and Preparation of P-DPD—P-DPD was produced enzymatically by the phosphorylation of DPD with purified LsrK and ATP. LsrK was purified as described previously (18). The reaction mixture contained 30 μg ml^{-1} LsrK, 2–3 mM DPD, 6 mM ATP, 24 mM $MgCl_2$, 100 mM potassium phosphate buffer pH 7.2, and 5% D_2O. Reaction mixtures were incubated at 30 °C for 10 min and terminated by placing the samples in ice. Typically, these conditions ensured a complete conversion of DPD to P-DPD, and this was always confirmed by ^{1}H NMR or ^{31}P NMR spectra (at 4 °C to avoid degradation).

LsrG Assays—To analyze the products of the LsrG reaction, 3 μg ml^{-1} final concentration of purified enzyme was added to the reaction mixture containing enzymatically prepared P-DPD. To ensure reducing conditions, samples were degassed with argon for 5 min, and freshly prepared DTT was added to a final concentration of 10 mM (unless mentioned otherwise) before the addition of LsrG. Incubation of these mixtures for 2 min at 30 °C was sufficient to ensure complete consumption of P-DPD. In cases where the LsrG reaction was performed in anaerobiosis, the LsrK reaction products were degassed by three cycles of vacuum and argon, and the LsrG enzyme and the diethylpyrocarbonate solution were left in an inert atmosphere glove box for 20 min. Mixtures were created in anaerobic conditions. To inhibit LsrG, diethylpyrocarbonate was used at a final concentration of 50 mM. The enzymatic activity of LsrG and its mutants was determined by monitoring the kinetics of P-DPD decrease at 30 °C by acquiring sequential ^{1}H NMR spectra (1.5 min each). For these experiments a batch of P-PDP was prepared as detailed above and quantified by ^{1}H NMR using formate as an internal reference. This mixture was kept in ice until use. Before each reaction an aliquot of 650 μl of the P-DPD sample was incubated for 5 min at 30 °C in a 5-mm NMR tube, and the reaction was started by adding the LsrG or its mutants

and placed in the spectrometer. The first spectra were started 1.5 min after enzyme addition. Controls with no enzyme or no substrate were performed for all conditions. To determine the specific enzyme activity, the concentration of protein added was adjusted to ensure that the rate of substrate consumption was linear at least in the first 10–12 min. For wild type (WT) LsrG, 1 μg ml^{-1} of protein was used, but for the point mutants, concentrations up to 20 μg ml^{-1} were tested.

Crystallization and Structure Determination

Crystals of WT LsrG with the His$_6$ tag removed were grown via the sitting drop method with a well solution of 1.65 M sodium citrate, pH 6.5. Crystals were cryoprotected in paratone and flash-frozen in the diffractometer cryostream. Data were collected at National Synchrotron Light Source beamline X25. The crystals (P$_{21}$, a = 44.64 Å, b = 83.39 Å, c = 63.59Å, β = 89.52°) diffracted to 1.8 Å resolution. Data were processed using Denzo, Scalepack, and CCP4 (24, 25).

The structure of LsrG was determined using molecular replacement with PHENIX (26) using LsrG from *Yersinia pestis* (Protein Data Bank ID 2GFF) as the search model. The model was rebuilt using Coot (27) and refined with PHENIX (26) and REFMAC (28). The model exhibits good geometry (Table 1), with no residues outside the allowed region of the Ramachandran plot. The final model includes 288 water molecules and has a final R_{cryst} of 0.204 and R_{free} of 0.240. Coordinates and structure factors for LsrG were deposited in the Protein Data Bank with accession number 3QMQ.

Structural alignments were calculated in Coot (27), and sequence alignments were calculated by ClustalW2 (29). All molecular images were generated using PyMOL (30).

Bacterial Strains, Plasmids, and Growth Conditions

All strains and plasmids used are listed in Table 2. These strains are all *E. coli* MG1655 derivatives of KX1123 ($\Delta lacZYA$, *lsr-lacZ* (14)). The strain JCM16 $\Delta lsrG$::Cm was constructed by replacing the *lsrG* gene in KX1123 by a chloramphenicol (Cm) resistance cassette as described previously (31) using primers with 50 bp of homology to the flanking regions of *lsrG* and was introduced in KX1123 by generalized transduction with bacteriophage P1 (32). To construct JCM23, Cm was removed from strain JCM16 with pcp20 as described (31). To obtain JCM62 ($\Delta lsrK$::Kan) a P1 lysate from the strain JW1504 $\Delta lsrK$::Kan (obtained from National BioResource Project (Japan):*E. coli*) was used to introduce this deletion into KX1123 by generalized P1 transduction. All plasmids were transformed by electroporation according to standard protocols (33). Except where otherwise stated, strains were grown in Luria-Bertani medium supplemented with 100 mM MOPS, pH 7, at 37 °C with shaking. Growth was monitored by optical density at 595 nm (A_{595}).

In Vivo Expression of Transcription of the lsr Operon

Expression of *lsr* transcription in *E. coli* was measured by determining the β-galactosidase activity of the *lsr-lacZ* promoter fusion as described before (14). To test the effect of the expression of LsrG and its mutants, the strains containing the pProExHTb plasmid and its derivatives were cultured in Luria-Bertani medium supplemented with 100 mM MOPS, pH 7.0, ampicillin (100 mg liter^{-1}) and isopropyl 1-thio-β-D-galactopyranoside (1 μg liter^{-1}). Isopropyl 1-thio-β-D-galactopyranoside was added 2.5 h after inoculation to mimic the start of *lsrG* induction in the WT strain. To assay β-galactosidase activity,

TABLE 1
Chrystallographic data and refinement statistics

Data collection[a]	
Resolution (Å)	1.80 (1.86-1.80)
Unique reflections	42,865 (4,284)
R_{merge}	0.127 (0.420)
Mean $I/\sigma I$	7.42 (1.99)
Completeness (%)	99.70 (99.80)
Multiplicity	3.6 (3.6)
Refinement	
R_{cryst}/R_{free}	0.204/0.243
r.m.s.d. bond length (Å)	0.023
r.m.s.d. bond angle (°)	1.97
No. of atoms per asymmetric unit	3,508
Average B factor (Å^2)	
Protein	19.68
Water	24.87
Ramachandran plot	
Most favored (%)	95.5
Allowed (%)	4.5
Disallowed (%)	0.0

[a] The highest resolution shell is shown in parenthesis.

TABLE 2
E. coli strains and plasmids used in this study

| Strains and plasmids	Relevant genotype	Source
***E coli* strains**		
KX1123	*lsr-lacZ, ΔlacZYA*	Xavier and Bassler (14)
KX1186	*lsr-lacZ, ΔlsrK::Tn10*Cm	Xavier and Bassler (14)
JCM16	*lsr-lacZ, ΔlsrG::*Cm	This study
JCM23	*lsr-lacZ, ΔlsrG*	This study
JCM43	*lsr-lacZ, ΔlsrG::*Cm, p*lsrG*-WT	This study
JCM44	*lsr-lacZ, ΔlsrG::*Cm, p*lsrG*-E54A	This study
JCM45	*lsr-lacZ, ΔlsrG::*Cm, p*lsrG*-H65A	This study
JCM46	*lsr-lacZ, ΔlsrG::*Cm, p*lsrG*-N25A	This study
JCM47	*lsr-lacZ, ΔlsrG::*Cm, pProExHtb	This study
JCM48	*lsr-lacZ, ΔlsrG::*Cm, p*lsrG*-H70A	This study
JCM53	*lsr-lacZ,* pProExHtb	This study
JCM62	*lsr-lacZ, ΔlsrK::*Kan, pProExHtb	This study
Plasmids		
pProExHTb	Expression vector with hexahistidine tag (Amp^R)	
p*lsrG*-WT	pProExHTb containing *lsrG*-WT	
p*lsrG*-E54A	pProExHTb containing *lsrG*-E54A	
p*lsrG*-H65A	pProExHTb containing *lsrG*-H65A	
p*lsrG*-N25A	pProExHTb containing *lsrG*-N25A	
p*lsrG*-H70A	pProExHTb containing *lsrG*-H70A	
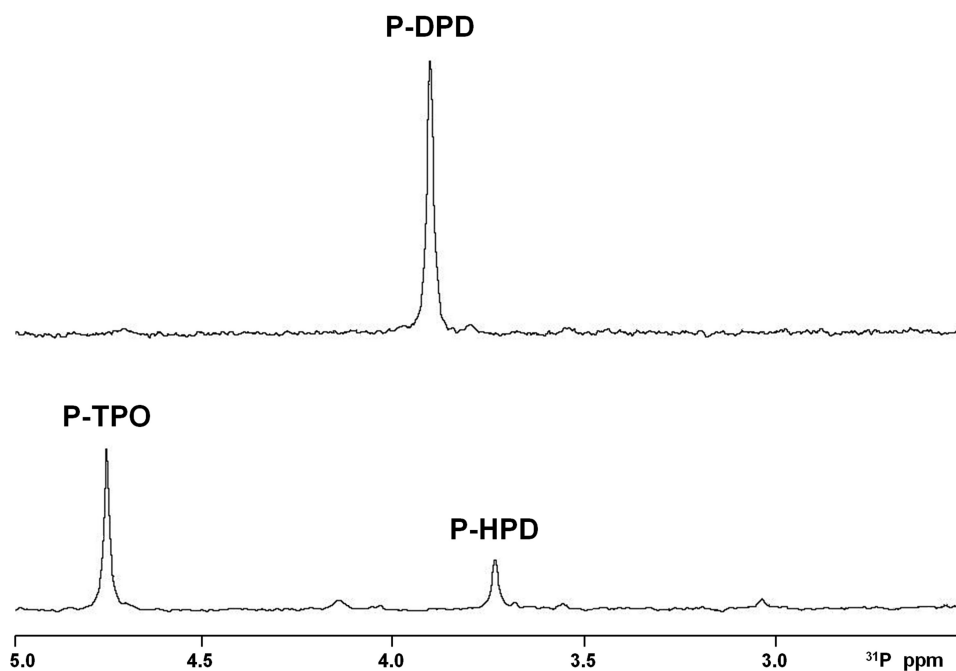
FIGURE 2. **^{31}P NMR spectra of P-DPD and the products of the LsrG reaction.** The *upper trace* shows the phosphorous resonance of P-DPD resulting from incubation of DPD with purified kinase (LsrK) and ATP. The *bottom trace* shows the phosphorous resonances of the products (*P-TPO* and *P-HPD*) after the addition of purified LsrG to the same reaction mixture in the presence of 10 mM DTT.

cells were collected and harvested when cultures reached $A_{595} = 3$. To measure *lsr-lacZ* expression in cell cultures during growth, extracts were created from 1 ml of culture aliquots collected in triplicate at the indicated times. All assays were performed in triplicate.

Time Course of AI-2 Production in Bacterial Cultures

To monitor extracellular AI-2 activity in cell cultures during growth, aliquots were collected at the indicated times and cell-free culture fluids were prepared by the filtration of liquid cultures (34, 35) and then analyzed for AI-2 activity. Quantification of AI-2 was performed using the *in vitro* assay based on the LuxP-FRET method established by Rajamani *et al.* (36) and optimized for 96-well plate reading using a multilabel counter (1420 Victor 3, PerkinElmer Life Sciences). Specifically, serial dilutions of sample were added to 12.5 μg ml^{-1} CFP-LuxP-YFP chimeric protein in 25 mM sodium phosphate buffer, pH 8, 35 mM NaCl, and 1 mM borate. Samples (2.5 μl) were added to a 280-μl reaction volume, and AI-2 concentrations of the samples were calculated from the FRET ratio (527/485 nm). Binding of AI-2 to the CFP-LuxP-YFP protein causes a dose-dependent decrease in the FRET signal, and concentration can be determined by comparing the FRET ratios of each sample with a calibration curve performed with AI-2 samples of known concentration produced and quantified as described in Schauder *et al.* (6). Concentrations between 1 and 60 μM AI-2 were used for the calibration curve, corresponding to the linear range of this assay. All assays were performed in triplicate.

Identification and Quantification of P-PDP in Cell Extracts

Each strain was cultured to $A_{595} = 3$ (conditions at which expression of *lsr* expression is high) and harvested by centrifugation at 7000 × g for 10 min at 4 °C. Cells were washed twice with 100 mM potassium phosphate buffer, pH 7.2, containing 1 mM MgCl$_2$; the cell pellets were resuspended in the same buffer and incubated with 2 mM DPD. After the addition of DPD, the cell suspension had a final volume of 3 ml and a calculated A_{595} of 70–80. This mixture was incubated at 30 °C with aeration. Efficient mixing and supply of oxygen to the cell suspension were achieved by bubbling oxygen and using an airlift system (37). After 15 min of incubation, ice-cold perchloric acid and DTT (0.6 M and 10 mM final concentrations, respectively) were added. The mixture was incubated for 20 min with stirring in an ice bath. 5 M KOH was then added to achieve pH 5. This extract was centrifuged for 15 min at 9000 × g at 4 °C. 5% D$_2$O, 5 mM EDTA, and 400 mM formate were added to the extracts for ^{1}H NMR analysis at 4 °C as described above.

RESULTS

LsrG Catalyzes Conversion of P-DPD to the Isomer P-TPO— When LsrG is incubated with P-DPD under reducing (*i.e.* in the presence of DTT) or anaerobic conditions, P-DPD is completely converted to two phosphorylated compounds as shown by ^{31}P NMR spectra (Fig. 2). The resonance at 4.75 ppm was assigned to the P-DPD isomer, P-TPO (Fig. 1, **3**), and the resonance with smaller intensity at 3.73 ppm was assigned to P-HPD (Fig. 1, **4**), the non-hydrated form of P-TPO. These compounds were identified by NMR spectroscopy, and the chemical shifts of the assigned resonances are summarized on Table 3. The ^{31}P resonances of the LsrG products are typical of phosphomonoester compounds, and their proton coupling patterns are triplets with coupling constants of 8.5 and 6.4 Hz for P-TPO and P-HPD, respectively. This pattern revealed that these two phosphate groups are linked to methylene groups. ^{1}H,^{31}P correlation experiments provided the chemical shifts of the resonances of the protons from the methylene groups asso-

TABLE 3
NMR parameters of P-DPD, P-TPO, P-HPD, P-TetraPO, and PG

^{13}C NMR δ (in ppm)	C-1	C-2	C-3	C-4	C-5
P-DPD (**2**)	27.2	212.6	99.2[a]	75.6	66.7
P-TPO (**3**)	31.4	216.0	81.0	98.6	69.1
P-HPD (**4**)	29.3	210.0	84.4	208.4	70.5
P-TetraPO (**5**)	29.2	213.3	99.9	98.2	68.4
PG[b]	181.0	66.1	-	-	-

^{31}P NMR δ (in ppm)	Phosphate
P-DPD (**2**)	3.90
P-TPO (**3**)	4.75
P-HPD (**4**)	3.73
P-TetraPO (**5**)	4.82
PG	2.88

^{1}H-NMR[c] δ (in ppm)	H-1	H-2	H-3	H-4	H-5a	H-5b
P-DPD (**2**)	2.37 (s)	-	-	4.11 (dd, 3.68, 6.93)	4.02 (m)	3.88 (dt, 11.34, 6.74)
P-TPO (**3**)	2.38 (s)	-	4.37 (s)	-	3.89 (t, 10.28)	3.76 (dd, 7.07, 11.19)
P-HPD (**4**)	2.35 (s)	-	ND[d]	-	4.78 (m)	4.64 (m)
P-TetraPO (**5**)	2.44 (s)	-	-	-	3.92 (d, 8.79)	3.92 (d, 8.79)
PG	-	4.17 (d, 5.21)	-	-	-	-

[a] This chemical shift shows that the P-DPD detected is hydrated at position 3.
[b] PG, phosphoglycolate.
[c] Multiplicities and coupling constants (Hz) are given in parentheses.
[d] ND, Not detected.

ciated with these phosphorous groups (Table 3, and supplemental Fig. S1, *lower panel*). Next we acquired a set of ^{13}C,^{1}H HMBC and ^{13}C,^{1}H HSQC NMR spectra to identify the other groups of these two compounds. In the assignment of P-TPO, the ^{13}C,^{1}H HMBC experiment (which correlates proton signals with neighboring carbon resonances two or three bonds apart) revealed that the protons from the phosphorylated carbon 5 of P-TPO, identified in the ^{1}H,^{31}P correlation experiments and labeled as 3_{H5a} and 3_{H5b} (Fig. 3) correlated with two carbon signals. Specifically, the chemical shift of the most intense correlation (at 98.6 ppm), assigned to carbon 4 (Fig. 3, $3_{H5a/b}/3_{C4}$), is consistent with a gem-diol, whereas the weaker correlation (at 81.0 ppm), assigned to carbon 3 (Fig. 3, $3_{H5a/b}/3_{C3}$), is typical of an alcohol group. We then used the ^{13}C,^{1}H HSQC spectrum (supplemental Fig. S2), which determines direct correlation between carbons and attached protons to determine the proton signal of carbon 3 from P-TPO (4.37 ppm). Again, in the ^{13}C,^{1}H HMBC spectrum, the proton bound to carbon 3 (Fig. 3, 3_{H3}) revealed a correlation with carbon 4 (identified above) and another at 216 ppm, identified as a carbonyl group assigned as carbon 2 (Fig. 3, $3_{H3}/3_{C2}$). This resonance from carbon 2 in turn is correlated with a proton resonance at 2.38 ppm in the methyl region (Fig. 3, $3_{H1}/3_{C2}$), which in the HSQC spectrum showed a correlation with a carbon at 31.4 pm assigned as carbon 1 (supplemental Fig. S2, Table 3). Overall, these data lead us to propose that the main product of the LsrG reaction (Fig. 1) is the compound P-TPO.

^{1}H NMR spectra of the reaction mixture, resulting from incubation of P-DPD with LsrG under reducing conditions, show two resonances in the methyl region: one at 2.38 ppm

assigned to P-TPO and a second one at 2.35 ppm with lower intensity (supplemental Fig. S3, *middle trace*). This result is consistent with the phosphorous spectrum mentioned above (Fig. 2). Given that the proton resonance at 2.35 ppm is present only when the weaker phosphorous resonance labeled as P-HPD in Fig. 2 is also present, we conclude that this methyl group and the phosphate group belong to the same compound, a conclusion supported by the relative intensities of the signals in the phosphorous and proton spectra (Fig. 2 and supplemental Fig. S3). Using a combination of ^{13}C,^{1}H HMBC (Fig. 3 and supplemental Fig. S1) and ^{13}C,^{1}H HSQC (supplemental Fig. S2) correlation spectra and following the strategy used for the assignment of P-TPO, we determined all the carbon resonances of this second compound (Table 3), allowing us to propose that this second compound is P-HPD (Fig. 1*A*, **4**). Although all the assignments are consistent with the proposed identification, we could not detect the correlation between carbon-4 or carbon-2 and proton-3 (supplemental Fig. S1), preventing us from firmly linking both ends of this compound. Importantly, all the carbon resonances assigned to P-HPD are very similar to P-TPO differing only in carbon 4, which is a ketone group (with a carbon resonance at 208.4 ppm) in P-HPD and a gem-diol (carbon resonance at 98.6 ppm) in P-TPO. Thus, P-TPO is the hydrated form of P-HPD position C4.

Production of P-TPO, **3,** from P-DPD, **2,** can be easily explained by the interconversion of the ketone at position C3 and the hydroxide at C4 from P-DPD, **2**, via the formation of 3,4-enediol intermediate to give the isomeric hydroxyketone, P-HPD, **4**, and then hydration at position C4 (Fig. 1*A*). The proposed keto-enol tautomerization is common in well charac-
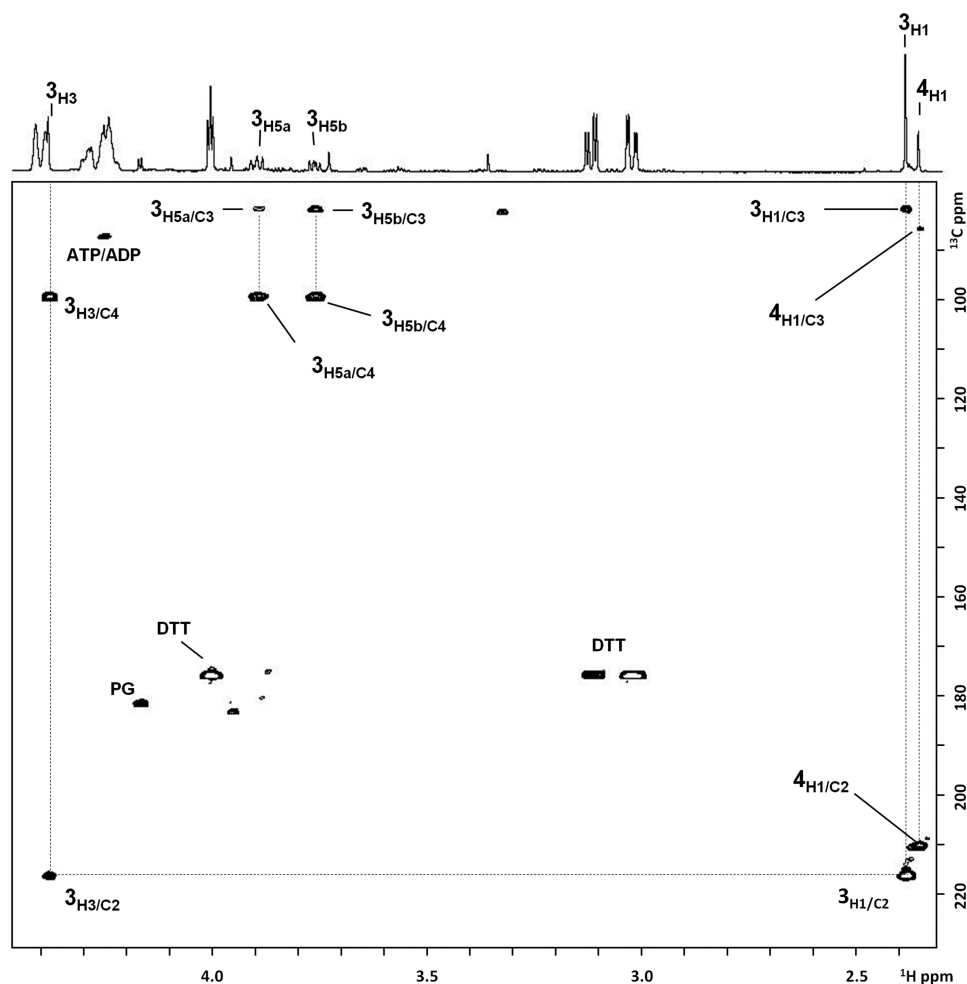
FIGURE 3. **³¹,¹H HMBC correlation spectrum of the products of the LsrG reaction.** The *upper trace* shows the ¹H NMR spectrum. The cross-peaks correspond to connectivities between proton and carbon atoms two or three bonds apart. *Dotted lines* highlight the most relevant correlations of the two products, P-TPO and P-HPD. The assignments are indicated next to each signal. Each relevant cross peak is labeled with **3** (for P-TPO) or **4** (for P-HPD) and *subscript with the letters H or C* for proton or carbon resonances, and the subsequent *numerals* represent the carbon group where 1 is the position of the methyl groups. Correlation of ATP/ADP, DTT, and phosphoglycolate (*PG*) is also labeled.

terized biochemical pathways, and such interconversion can occur spontaneously with any general α-hydroxyketone but is usually slow in the absence of a suitable catalyst (38). Furthermore, such ketone groups are often in equilibrium with their hydrated forms (39). This is also consistent with our NMR data and strengthens the conclusion that the minor product of the LsrG reaction is P-HPD, the non-hydrated form of P-TPO in Fig. 1*A*. In this particular case the hydrated molecule is the predominant form. Thus, based on the proposed reaction for formation of P-TPO (summarized in Fig. 1*A*), we conclude that LsrG catalyzes the isomerization of P-DPD.

P-TPO Is Highly Susceptible to Spontaneous Oxidation— When the LsrG/P-DPD reaction is performed in aerobic conditions and the absence of reducing agents, the products observed are P-TPO, P-HPD, P-TetraPO, phosphoglycolate, and other minor compounds (proton and phosphorous spectra, supplemental Fig. S3 and S4, respectively). The product P-TetraPO was assigned using a combination of proton, carbon, and phosphorous correlation NMR techniques as explained above (resonances are listed in Table 3). Phosphoglycolate had been previously assigned (18). The low concentrations of the other compounds precluded reliable identification by NMR.

Our results further showed that P-TetraPO and the other compounds mentioned above are produced from oxidation of P-TPO and P-HPD (supplemental Fig. S3, *panel B*). To determine whether this reaction is catalyzed by LsrG, we took advantage of the fact that diethylpyrocarbonate completely inhibits LsrG activity (data not shown). We measured the conversion of P-TPO and P-HPD into P-TetraPO in the presence of diethylpyrocarbonate or in its absence after bubbling oxygen through these samples. The decrease of P-TPO and P-HPD and the increase of P-TetraPO was very similar in both cases (supplemental Fig. S5), and thus we concluded that production of P-TetraPO does not require LsrG activity. It is also important to note that phosphoglycolate production was increased in the presence of oxygen; this could be due to the breakdown of P-TetraPO or the breakdown of P-TPO and P-HPD, but we have not pursued this issue. Additionally, as reported before (18) phosphoglycolate is also formed from P-DPD in the absence of LsrG, presumably as a result spontaneous degradation of P-DPD. We never observed the formation of P-TPO or P-HPD in the absence of LsrG. These data corroborate the conclusion that LsrG catalyzes the isomerization of P-DPD to P-TPO, which is in equilibrium with its non-hydrated form,
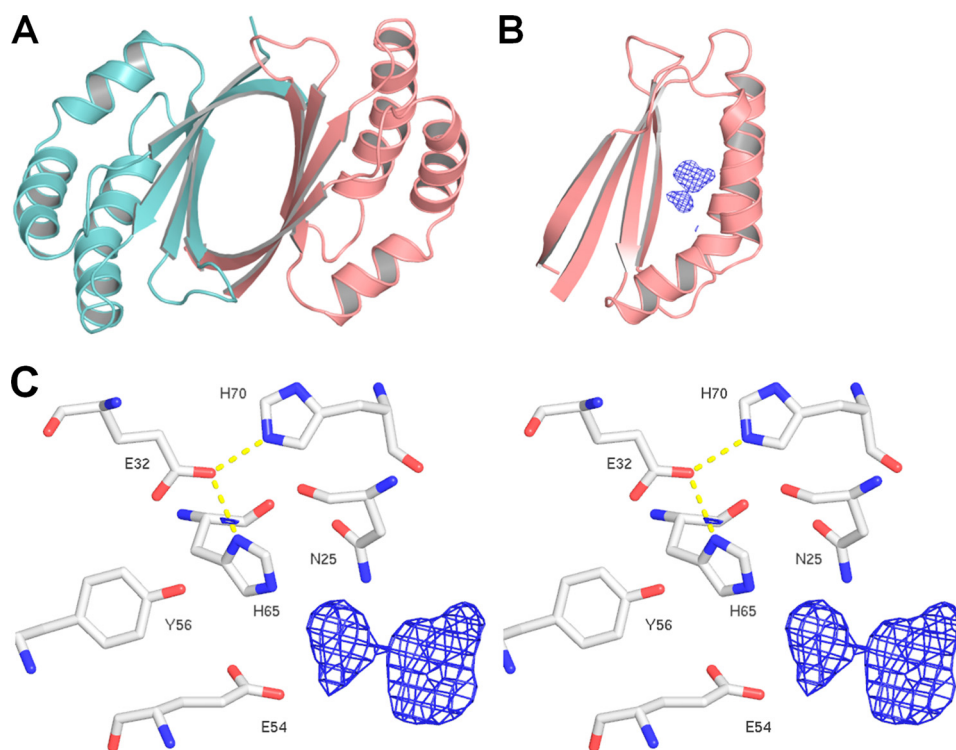
FIGURE 4. **Structure and predicted binding site of LsrG.** *A*, shown is a schematic representation of the LsrG dimer. *B*, a schematic representation of a LsrG monomer shows the location of non-protein density in the putative active site. Density is 4-fold NCS averaged, contoured at 4.0 σ, and truncated at 5.0 Å from the putative active site residues Glu-54 and Leu78. *C*, shown is a stereoview of key residues near the non-protein density. Density was prepared as in *B*.

P-HPD, and that in the presence of oxygen these compounds are oxidized non-enzymatically to produce P-TetraPO, phosphoglycolate, and other minor compounds.

Crystal Structure of LsrG and Implications for Catalysis—To investigate the catalytic mechanism of LsrG, we determined the crystal structure of *E. coli* LsrG to 1.8 Å resolution. The crystal structure revealed that LsrG is a dimeric $\alpha+\beta$ barrel (Fig. 4*A*). After building the protein structure, it became apparent that a large mass of non-protein electron density was present in a groove between the α-helices and β-strands of each subunit. We were unable to interpret this density either manually or using the ligand identification module in Phenix (26). Nonetheless, the location of this non-protein electron density suggests a possible location for the LsrG active site (Fig. 4*B*). Examination of this putative active site reveals several potential catalytic residues with side chains adjacent to the non-protein density, including Asn-25, Glu-54, and His-65 (Fig. 4*C*). His-70 might also be significant, acting to position His-65 properly.

A DALI search of the Protein Data Bank identified several close structural homologues including YgiN (1.7 Å r.m.s.d., 16% ID), SnoaB (1.8 Å r.m.s.d., 18% ID), ActVA-Orf6 (2.3 Å r.m.s.d., 17% ID), and IsdG (2.5 Å r.m.s.d., 16% ID) as well as a variety of hypothetical or uncharacterized proteins (40). All of these homologues have monooxygenase activity, but they act on a variety of substrates and in a range of pathways from antibiotic synthesis to heme degradation (for review, see Ref. 20). Interestingly, when LsrG is structurally aligned with these proteins, the observed non-protein density closely aligns with the active sites of each, further supporting the assignment of this region as the active site in LsrG.

Examination of the active sites shows very little conservation of catalytic residues between LsrG and its structural homologues. Most notably, a tryptophan residue (Trp-66 in ActVA-Orf6) that is conserved in the other homologues is replaced by a tyrosine (Tyr-56) in LsrG. In the monooxygenases this conserved tryptophan has been implicated in substrate specificity (ActVA-Orf6 (21), YgiN (41), SnoaB (42)) and may play a role in catalysis; the fact it is not conserved in LsrG suggests a significantly different substrate or, potentially, a different functionality for this enzyme. Other active site residues from these proteins are not generally conserved in LsrG, although there is modest conservation with YgiN, the closest homologue (41). Of the residues that Adams and Jia (41) suggest could play a catalytic role in YgiN, only His-75 is structurally conserved (His-65 in LsrG). His-65 is one of the residues we identified as potentially catalytic in LsrG (above); one of the others, Glu-54, is also conserved in YgiN (Glu-64).

Sequence Comparison with LsrG from Other Organisms—In earlier work (12) we used bioinformatics analysis to identify bacterial species that have a functional *lsr* operon. Using the sequences for LsrG from these species, we created a multiple sequence alignment via ClustalW2 (29). Only nine residues are completely conserved across all species (in addition to the start Met), and of these, only two residues (Gly-34 and Asp-39) are not positioned near the putative active site. These residues are likely conserved for structural reasons; Asp-39, in particular, is positioned near the dimer interface and forms hydrogen bonds with Arg-37 in the other chain.

Of the other seven residues, two (Glu-54 and His-65) are directly adjacent to the putative ligand density as shown in Fig.

TABLE 4

Specific enzyme activities of LsrG-WT and single amino acid mutants: E54A, H65A, N25A, and H70A

Protein	Activities
	Units/mg of protein[a]
LsrG-WT	61.0 ± 2.2
LsrG-E54A	< 0.1
LsrG-H65A	< 0.1
LsrG-N25A	20.4 ± 0.8
LsrG-H70A	0.8 ± 0.1

[a] One unit of enzyme activity is defined as 1 μmol of P-DPD consumed/min at 30 °C.

FIGURE 5. **The effect of *lsrG* and its mutants on the *lsr* expression in *E. coli*.** β-Galactosidase activity of the *lsr-lacZ* transcription reporter fusion was measured in WT and $\Delta lsrG$ strains expressing pProExHTb (empty vector). Activity was also measured in $\Delta lsrG$ strains carrying the pProExHTb with wild type *lsrG* (*lsrG*-WT) or the *lsrG* single amino acid alanine substations *lsrG* mutants E54A, H65A, N25A, and H70A. The *error bars* indicate S.D.

4*C* and mentioned above. The position of these residues coupled with the fact that they are conserved across species suggests that they are likely to play catalytic roles. The remaining residues are in or around the active site and may play roles in determining the geometry of the active site. His-70 is positioned to form a hydrogen bond with Glu-32, which in turn forms a hydrogen bond with His-65. Val-75 is directly adjacent to the putative ligand density but, given its hydrophobic nature, is unlikely to be directly catalytic. Phe-18 may be involved in a stacking interaction with two other Phe residues, one of which (Phe-22) is directly adjacent to the active site. Asn-35 is adjacent to Tyr-56, a residue notable for occupying the position of the tryptophan residue widely conserved in the monooxygenases. Thus, the complete conservation of putative catalytic residues and the positioning of the other conserved residues support our identification of the LsrG active site.

Site-directed Mutagenesis of the LsrG and Impact on Enzyme Activity and Activation of lsr Transcription—Based on the location of the putative active site in the crystal structure and the analysis of sequence alignments (above), we identified four residues (Glu-54, His-65, Asn-25, and His-70) most likely to play a major role in catalysis. To test these four residues for a catalytic role, we generated individual alanine substitution mutants and tested these mutants (E54A, H65A, N25A, and H70A) for enzymatic activity *in vitro* using purified protein and *in vivo* via *lsrG* expressed from multicopy plasmids in an *lsrG* deletion mutant. As shown in Table 4, mutants E54A, H65A, and H70A had no or very low activity *in vitro*, and the N25A mutant had a significant reduced activity (about 3-fold less activity than WT). For the *in vivo* assays, we used a strain with a *lsr-lacZ* transcriptional reporter fusion because transcription of the *lsr* operon is activated by P-DPD (14, 17). The WT strain has lower *lsr-lacZ* activity than the *lsrG* deletion mutant (*two first bars*, Fig. 5) presumably because the absence of *lsrG* results in P-DPD accumulation. Accordingly, complementing the mutant with an isopropyl 1-thio-β-D-galactopyranoside-inducible multicopy plasmid expressing the *lsrG*-WT gene caused a reduction in *lsr-lacZ* activity (*third bar*, Fig. 5). We compared the ability of the plasmids expressing *lsrG*-WT to induce *lsr* transcription with that of plasmids expressing the single point mutants. In agreement with the *in vitro* results, ectopic expression from the plasmids containing E54A, H65A, or H70A *lsrG* did not complement the effect of the *lsrG* deletion on *lsr* transcription. However, complementation with plasmid carrying the N25A mutant was as effective as with plasmid containing *lsrG*-WT (Fig. 5). This correlates with *in vitro* result where N25A shows detectable activity. Although the activity *in vitro* is still lower
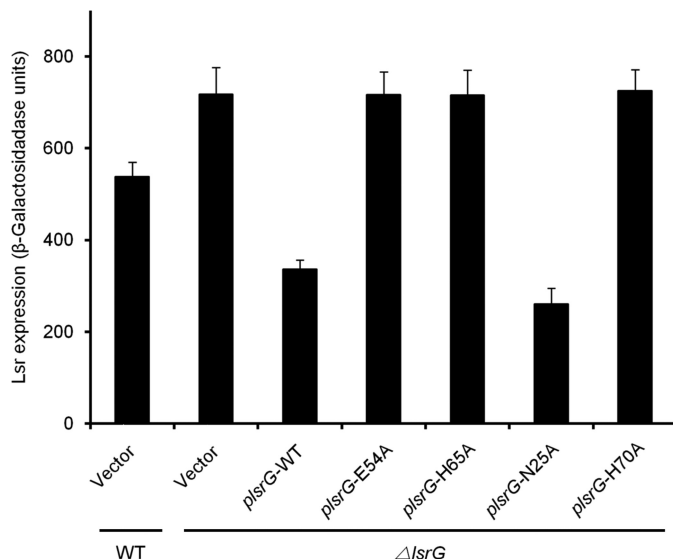
than in WT, this difference is not observed in our *in vivo* system. These data show that the N25A mutant is slightly catalytically impaired, suggesting that Asn-25 plays a role in catalysis but that the catalytic defect can be overcome by expression from a multi-copy isopropyl 1-thio-β-D-galactopyranoside-inducible plasmid with the resulting higher concentration of protein in the cell.

Impact of LsrG on Intracellular AI-2-P Accumulation—Previous work showed that the *lsr* operon is mainly induced by P-DPD, and thus the fact that expression of the *lsr* operon in an *lsrG* mutant is higher than in the WT leads to the suggestion that the mutant accumulates more P-DPD than the WT (17). If this is the case, overexpression of plasmid-borne *lsrG* in this mutant would prevent this accumulation. To test this hypothesis, we measured the accumulation of P-DPD in cell extracts of the following *E. coli* strains: WT, the *lsrG* deletion mutant, and the mutant complemented with p*lsrG*-WT. The levels of free P-DPD were determined by proton NMR of extracts from cell suspensions actively metabolizing DPD. P-DPD was easily detected in the *lsrG* deletion mutant (P-DPD = 0.16 mM) but not in the other extracts (Fig. 6). Apparently, the rate of turnover of P-DPD in the strain overexpressing p*lsrG*-WT and even in the WT strain is sufficiently high that the P-DPD level was below our detection limits (*i.e.* lower than 0.01 mM). As a negative control we assayed cell extracts from the *lsrG* mutant when no DPD was added to the cell suspension, and as expected, no resonance with the P-DPD chemical shift was detected (Fig. 6, *lower trace*). A mutant in the kinase that phosphorylates DPD (*lsrK*) was used as an additional negative control, and again, no P-DPD was detected (Fig. 6). This direct measurement of P-DPD levels supports the earlier prediction that the increase in *lsr* transcription observed in *lsrG* mutants is a result of P-DPD accumulation.
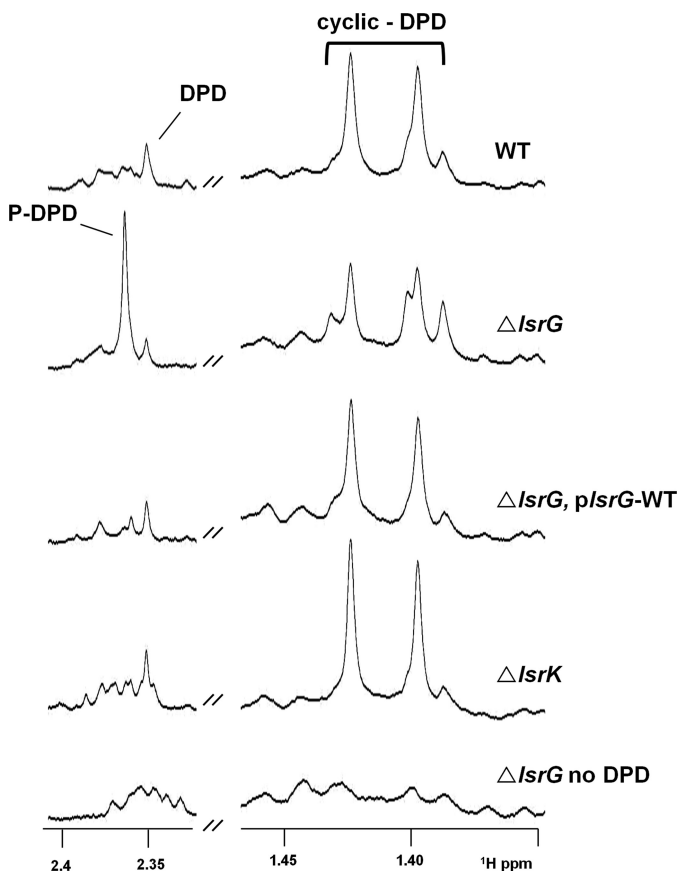
FIGURE 6. **P-DPD accumulation in *E. coli* cell suspensions metabolizing DPD.** The methyl region of the ^{1}H NMR spectra of cell extracts from different *E. coli* strains is shown. Each trace shows the spectrum of the extract obtained from strains: JCM53 (WT + pProExHTb), JCM47 (ΔlsrG + pProExHTb), JCM43 (ΔlsrG + plsrG-WT), and JCM62 (ΔlsrK + pProExHTb) from *top to bottom*. Extracts were obtained from cell suspensions incubated at 30 °C for 15 min with 2 mM DPD (except for the *lower trace* (strain JCM47) to which no DPD was added). Cell extracts were performed as described under "Experimental Procedures." The relevant genotype of the strains used in each case is indicated next to the trace. The resonances of the methyl groups from P-DPD and the three forms of DPD are highlighted.

Impact of LsrG Mutation on Accumulation of Extracellular AI-2 in Vivo—In cultures of WT *E. coli* in Luria-Bertani medium, extracellular AI-2 concentration typically increases over time up to 30–40 μM and then begins to decline to undetectable levels (Fig. 7A, *circles*). This profile correlates with the timing of activation of *lsr* transcription (Fig. 7B, *circles*) and, presumably, the Lsr-mediated transport of AI-2 into the cells. In contrast, in an *lsrK* mutant, AI-2 is not phosphorylated; thus, transcription of the *lsr* operon is not induced, and extracellular AI-2 levels remain high (Fig. 7, *squares*). In the *lsrG* mutant (Fig. 7, *triangles*), AI-2 internalization starts at lower concentration of extracellular AI-2 (15–20 μM) and, accordingly, induction of *lsr* transcription starts earlier and reaches levels higher than the WT. This is in agreement with our conclusion that *lsrG* mutants accumulate higher levels of the *lsr* inducer P-DPD (Fig. 6). Nonetheless, we were surprised that the extracellular levels of AI-2 in this mutant stop decreasing after a fast initial decrease. We hypothesize that accumulation of P-DPD causes feedback inhibition of the LsrK kinase, and as a consequence, non-phosphorylated AI-2 can exit the cell and accumulate in the medium.

DISCUSSION

P-DPD is the intracellular inducer of the *lsr* operon, the gene products of which form a system capable of terminating AI-2-mediated bacterial behaviors (11, 43). Using NMR, x-ray crystallography, and a combination of *in vitro* and *in vivo* assays, we showed that LsrG catalyzes the isomerization of P-DPD to P-TPO (and its non-hydrated form, P-HPD). Our finding was surprising given our previous report (18), but it is not inconsistent. We had suggested that LsrG catalyzes the cleavage of P-DPD to phosphoglycolate and other unknown products. The experiments reported here show that the increased formation of phosphoglycolate observed in the presence of LsrG occurs only when the products of P-DPD isomerization are exposed to oxidative conditions. In the presence of oxygen, P-TPO and P-HPD are oxidized to P-TetraPO, phosphoglycolate, and other minor compounds, but this oxidation does not require active LsrG. Under anaerobic conditions we never observed formation of P-TetraPO or phosphoglycolate. Additionally, we also never observe these two compounds when the reaction is preformed in the presence of the reducing agents DTT or glutathione (supplemental Figs. S6 and S7). Overall, our results indicate that the physiological function of LsrG is to catalyze P-DPD isomerization. Whether or not the products of this reaction are oxidized to phosphoglycolate *in vivo* will depend on the local oxidizing/reducing conditions and, potentially, the efficiency of other enzymes that act on the P-DPD isomers, and this is a question we are pursuing through ongoing experiments. To completely reveal the metabolic fate of DPD, it is necessary to identify and characterize the next steps of this pathway. The answer will provide clues to other benefits the bacteria may derive from the processing of DPD, metabolic or otherwise.

Using NMR to measure the accumulation of P-DPD in extracts of cells actively metabolizing DPD, we showed that the *lsrG* deletion mutant accumulates at least 10 times more P-DPD than WT. This assay provides a novel and direct way to measure intracellular P-DPD and can be applied to the study of other enzymes involved in P-DPD processing or regulators of this process. In this particular case, this observation provided direct evidence on the impact of *lsrG in vivo* and explains the high levels of Lsr expression observed in this mutant. Our results also showed that the *lsrG* deletion mutant has an aberrant profile of AI-2 internalization. Thus, LsrG is essential for the proper functioning of the Lsr system in interfering with AI-2-mediated signaling.

The crystal structure of P-DPD showed that LsrG has the same fold as enzymes belonging to the cofactor-independent monooxygenase family such as ActVA-Orf6, YgiN, and SnoaB (21, 41, 42). However, our data indicate that, unlike the other enzymes from this family, LsrG does not catalyze the incorporation of oxygen into the substrate; thus, LsrG plays a different catalytic role than other members of the family characterized so far. It is notable, however, that the keto-enol tautomerization step we propose for the LsrG reaction is also a step in the pathway of ActVA-Orf. Thus, the isomerization catalyzed by LsrG could be setting the stage for the oxidation reaction that leads to the observed production of P-TetraPO and phosphoglycolate.
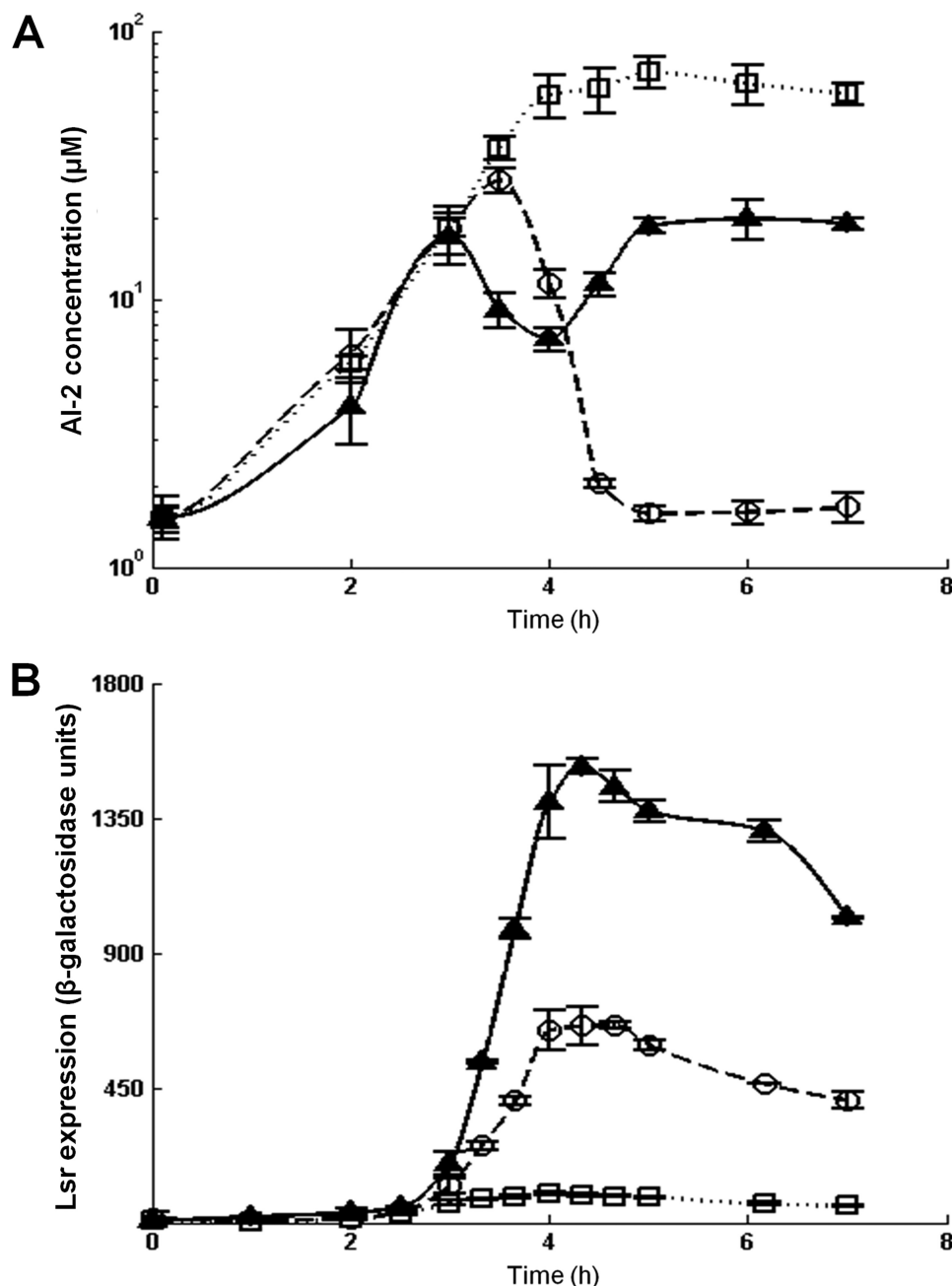
FIGURE 7. **Profile of extracellular AI-2 accumulation and expression of *lsr* during growth.** Extracellular AI-2 (*A*) and β-galactosidase activity of the *lsr-lacZ* transcription reporter fusion (*B*) were measured in WT (MG1655, *circles*), ΔlsrK (KX1186, *squares*), and ΔlsrG (JCM23, *triangles*) *E. coli* strains. Measurements were performed on aliquots collected at indicated times. The *error bars* indicate S.D.

Whether this oxidation occurs *in vivo* remains an open question.

Identification of the crystal structure led us to identify potential catalytic residues, and we assayed mutants of these sites. Our results showed that the residues Glu-54, His-65, and His-70 are essential for catalysis *in vitro* and that alanine substitutions of these residues are impaired in complementing the *lsrG* deletion mutant *in vivo*. These catalytic residues from LsrG are not structurally conserved in other proteins from the monooxygenase family studied so far. The same is largely true between the catalytic residues of other members of this family and can be explained by divergent adaptation to a variety of substrates (20, 42). One exception is the residue His-65, which

is structurally conserved in YgiN (His-75), the closest structural homologue to LsrG, and demonstrated to be important for catalysis in both LsrG and YgiN (41).

Although the conservation of catalytic residues among the proteins from this family is low, this is not the case among the previously identified LsrG orthologs (12). In this group there was 100% conservation of 7 residues in and around the active site (which include the residues Glu-54 and His-65 and His-70) out of a total of only 9 completely conserved residues (in addition to the start Met). Asn-25, which is close to the potential active site, is only conserved in 17% of these proteins, suggesting that it plays a non-essential role in support of LsrG catalysis. This is in line with experimental results showing

reduced activity for the N25A mutant *in vitro* (though not *in vivo*, see above). The conservation of other active site residues, including those shown here to be essential for function, supports the prediction that the function of LsrG in the regulation of the Lsr system is conserved in the range of species with LsrG homologues. The *lsr* operon and *lsrG* homologues are present in bacteria including important human pathogens such as *S. typhimurium, B. anthracis,* and *Y. pestis* (12) and thus can impact communications in multispecies bacterial communities that include pathogens such as these.

The belief in the field is that quorum sensing can be exploited to manipulate bacterial behavior and thus lead to an alternative to traditional antibiotics. This is mainly because therapies that interfere with quorum sensing are predicted to create lower selective pressure toward resistance than traditional anti-microbial treatments (44, 45). A variety of approaches are being developed that interfere at different steps on the quorum-sensing pathways. One of these strategies, referred to as quorum quenching, involves altering or destroying the autoinducer signal (46). Most reports on quorum-quenching approaches have employed naturally occurring enzymes that degrade species-specific signals. Enzymes that degrade acylhomoserine lactones (AHLs) include AHL lactonases (47), AHL acylases (48), and paraoxonases (49). Fewer studies have investigated interference with autoinducer peptides, but examples of quorum-sensing inhibition in *Staphylococcus aureus* are reviewed in Lyon and Novick (50). In contrast, the Lsr system and LsrG in particular targets the interspecies signal AI-2. This is the only natural system known so far to degrade AI-2 signal, and there are already multiple studies showing that the Lsr system can function as an AI-2 quenching system (11, 43). Our work shows that interference with LsrG alters the function of Lsr, suggesting that it could be a useful target for AI-2-based quorum-quenching therapies. Interference with interspecies cell-cell signaling can be particularly important when treating infections caused by multispecies biofilms that might rely on interspecies signals for persistence. For these cases, we predict that targeting interspecies signaling is likely to be more effective than targeting species-specific signals.

REFERENCES

1. Waters, C. M., and Bassler, B. L. (2005) *Annu. Rev. Cell Dev. Biol.* **21,** 319–346
2. Ng, W. L., and Bassler, B. L. (2009) *Annu. Rev. Genet.* **43,** 197–222
3. Bassler, B. L., Greenberg, E. P., and Stevens, A. M. (1997) *J. Bacteriol.* **179,** 4043–4045
4. Xavier, K. B., and Bassler, B. L. (2003) *Curr. Opin. Microbiol.* **6,** 191–197
5. Federle, M. J. (2009) *Contrib. Microbiol.* **16,** 18–32
6. Schauder, S., Shokat, K., Surette, M. G., and Bassler, B. L. (2001) *Mol. Microbiol.* **41,** 463–476
7. Chen, X., Schauder, S., Potier, N., Van Dorsselaer, A., Pelczer, I., Bassler, B. L., and Hughson, F. M. (2002) *Nature* **415,** 545–549
8. Miller, S. T., Xavier, K. B., Campagna, S. R., Taga, M. E., Semmelhack, M. F., Bassler, B. L., and Hughson, F. M. (2004) *Mol. Cell* **15,** 677–687
9. Vendeville, A., Winzer, K., Heurlier, K., Tang, C. M., and Hardie, K. R. (2005) *Nat. Rev. Microbiol.* **3,** 383–396
10. Hardie, K. R., and Heurlier, K. (2008) *Nat. Rev. Microbiol.* **6,** 635–643
11. Xavier, K. B., and Bassler, B. L. (2005) *Nature* **437,** 750–753
12. Pereira, C. S., de Regt, A. K., Brito, P. H., Miller, S. T., and Xavier, K. B. (2009) *J. Bacteriol.* **191,** 6975–6987
13. Taga, M. E., Semmelhack, J. L., and Bassler, B. L. (2001) *Mol. Microbiol.* **42,** 777–793
14. Xavier, K. B., and Bassler, B. L. (2005) *J. Bacteriol.* **187,** 238–248
15. Pereira, C. S., McAuley, J. R., Taga, M. E., Xavier, K. B., and Miller, S. T. (2008) *Mol. Microbiol.* **70,** 1223–1235
16. Wang, L., Li, J., March, J. C., Valdes, J. J., and Bentley, W. E. (2005) *J. Bacteriol.* **187,** 8350–8360
17. Taga, M. E., Miller, S. T., and Bassler, B. L. (2003) *Mol. Microbiol.* **50,** 1411–1427
18. Xavier, K. B., Miller, S. T., Lu, W., Kim, J. H., Rabinowitz, J., Pelczer, I., Semmelhack, M. F., and Bassler, B. L. (2007) *ACS Chem. Biol.* **2,** 128–136
19. Xue, T., Zhao, L., Sun, H., Zhou, X., and Sun, B. (2009) *Cell Res.* **19,** 1258–1268
20. Fetzner, S., and Steiner, R. A. (2010) *Appl. Microbiol. Biotechnol.* **86,** 791–804
21. Sciara, G., Kendrew, S. G., Miele, A. E., Marsh, N. G., Federici, L., Malatesta, F., Schimperna, G., Savino, C., and Vallone, B. (2003) *EMBO J.* **22,** 205–215
22. Ascenso, O. S., Marques, J. C., Santos, A. R., Xavier, K. B., Ventura, M. R., and Maycock, C. D. (2011) *Bioorg. Med. Chem.* **19,** 1236–1241
23. Shaka, A. J., Barker, P. B., and Freeman, R. (1985) *J. Magn. Reson.* **64,** 547–552
24. Otwinowski, Z., and Minor, W. (1997) *Processing of X-ray Diffraction Data Collected in Oscillation Mode*, pp. 307–326, Academic Press, Inc., Orlando, FL
25. CCP4 (1994) *Acta Crystallogr. D Biol. Crystallogr.* **50,** 760–763
26. Adams, P. D., Afonine, P. V., Bunkóczi, G., Chen, V. B., Davis, I. W., Echols, N., Headd, J. J., Hung, L. W., Kapral, G. J., Grosse-Kunstleve, R. W., Mc-Coy, A. J., Moriarty, N. W., Oeffner, R., Read, R. J., Richardson, D. C., Richardson, J. S., Terwilliger, T. C., and Zwart, P. H. (2010) *Acta Crystallogr. D Biol. Crystallogr.* **66,** 213–221
27. Emsley, P., and Cowtan, K. (2004) *Acta Crystallogr. D Biol. Crystallogr.* **60,** 2126–2132
28. Murshudov, G. N., Vagin, A. A., and Dodson, E. J. (1997) *Acta Crystallogr. D Biol. Crystallogr.* **53,** 240–255
29. Chenna, R., Sugawara, H., Koike, T., Lopez, R., Gibson, T. J., Higgins, D. G., and Thompson, J. D. (2003) *Nucleic Acids Res.* **31,** 3497–3500
30. DeLano, W. L. (2010) *The PyMOL Molecular Graphics System*, Version 1.3r1, Schrodinger, LLC, New York
31. Datsenko, K. A., and Wanner, B. L. (2000) *Proc. Natl. Acad. Sci. U.S.A.* **97,** 6640–6645
32. Silhavy, T. J., Berman, M. L., and Enquist, L. W. (1984) *Experiments with Gene Fusions*, pp. 107–111, Cold Spring Harbor Laboratory, Cold Spring Harbor, New York
33. Sambrook, J., Fritsch, E. F., and Maniatis, T. (2001) *Molecular Cloning: A Laboratory Manual*, 3rd Ed., pp. 1.119–1.122, Cold Spring Harbor Laboratory, Cold Spring Harbor, New York
34. Surette, M. G., and Bassler, B. L. (1999) *Mol. Microbiol.* **31,** 585–595
35. Surette, M. G., and Bassler, B. L. (1998) *Proc. Natl. Acad. Sci. U.S.A.* **95,** 7046–7050
36. Rajamani, S., Zhu, J., Pei, D., and Sayre, R. (2007) *Biochemistry* **46,** 3990–3997
37. Santos, H., and Turner, D. L. (1986) *FEBS Lett.* **194,** 73–77
38. Matheus, C. K., Van Holde, K. E., and Ahern, K. G. (1999) *Biochemistry*, 3rd Ed., p. 280, Addison Wesley Longman, Inc., San Francisco, CA

39. Damitio, J., Smith, G., Meany, J. E., and Pocker, Y. (1992) *J. Am. Chem. Soc.* **114,** 3081–3087

40. Holm, L., and Rosenström, P. (2010) *Nucleic Acids Res.* **38,** W545–W549

41. Adams, M. A., and Jia, Z. (2005) *J. Biol. Chem.* **280,** 8358–8363

42. Grocholski, T., Koskiniemi, H., Lindqvist, Y., Mäntsälä, P., Niemi, J., and Schneider, G. (2010) *Biochemistry* **49,** 934–944

43. Roy, V., Fernandes, R., Tsao, C. Y., and Bentley, W. E. (2010) *ACS Chem. Biol.* **5,** 223–232

44. Lowery, C. A., Dickerson, T. J., and Janda, K. D. (2008) *Chem. Soc. Rev.* **37,** 1337–1346

45. Rasko, D. A., and Sperandio, V. (2010) *Nat. Rev. Drug Discov.* **9,** 117–128

46. Dong, Y. H., Wang, L. Y., and Zhang, L. H. (2007) *Philos. Trans. R. Soc. Lond B. Biol. Sci.* **362,** 1201–1211

47. Dong, Y. H., Wang, L. H., Xu, J. L., Zhang, H. B., Zhang, X. F., and Zhang, L. H. (2001) *Nature* **411,** 813–817

48. Leadbetter, J. R., and Greenberg, E. P. (2000) *J. Bacteriol.* **182,** 6921–6926

49. Yang, F., Wang, L. H., Wang, J., Dong, Y. H., Hu, J. Y., and Zhang, L. H. (2005) *FEBS Lett.* **579,** 3713–3717

50. Lyon, G. J., and Novick, R. P. (2004) *Peptides* **25,** 1389–1403

Access the most updated version of this article at doi: 10.1074/jbc.M111.230227

Alerts:

- When this article is cited
- When a correction for this article is posted

Click here to choose from all of JBC's e-mail alerts

Supplemental material:

http://www.jbc.org/content/suppl/2011/03/30/M111.230227.DC1

This article cites 45 references, 10 of which can be accessed free at
http://www.jbc.org/content/286/20/18331.full.html#ref-list-1